Journal of Shipping and Ocean Engineering 11 (2021) 1-15
Doi: 10.17265/2159-5879/2021.01.001

# Effect of Freshwater Forcing on the Biogeochemistry of the Bay of Bengal

Saswati Deb[1], Arun Chakraborty[2], and Bhaskar Das[3]

*1. Fisheries and Oceans Canada, Gulf Fisheries Centre, New Brunswick, Canada*

*2. Centre for Oceans, Rivers, Atmosphere and Land Sciences, Indian Institute of Technology, Kharagpur, India*

*3. Département d'informatique, Université de Moncton, Moncton, New Brunswick, Canada*

**Abstract:** We developed a coupled 3-D physical-biogeochemical model for the Bay of Bengal (BoB) to simulate the seasonal variation of plankton dynamics to freshwater forcing using Regional Ocean Modeling System. Satellite-derived chlorophyll concentrations are assimilated using the OA method and SOR algorithm for the model input. To better understand the response of plankton dynamics to freshwater forcing two numerical experiments are conducted: 1) model run with freshwater discharges and applied physical-biogeochemical properties as Exp1; 2) model run without freshwater discharge but applying same physical-biogeochemical properties as Exp2. Intensification of bloom is marked on the western coast of the BoB during August-September due to increased nutrient supply from runoff apart from wind-driven upwelling, whereas in the eastern coast, two peaks of plankton biomass are observed in March followed by September. However, seasonal offshore plankton biomasses observed in the open and southern part of the BoB are potentially to linked with upwelling, entrainment-detrainment events and advection processes. Sensitivity experiments are also performed based on Exp1, by doubling the freshwater discharge in Exp1-FDD, which increased the bloom biomass by 60-65 percent; halved in Exp1-FDH reduced the bloom biomass by 25-15 percent signifies that the freshwater plays a dominant role along the coast but nonlinearly related to plankton dynamics.

**Key words:** Coupled physical-biogeochemical model, freshwater discharge, chlorophyll concentration, BoB, plankton dynamics.

## 1. Introduction

The Bay of Bengal (BoB) is a semi-enclosed basin (Fig. 1a) partly joined to the Pacific Ocean and the South China Sea through the Malacca Strait and Australasian seaways in the east, the Arabian Sea in the southwest and the Indian Ocean in the south. The Hooghly estuary in the north and other significant estuaries along the coast of the BoB are noteworthy for their biophysical exchanges. The distinctive biophysical features of BoB and seasonal variability have led researchers to study and explore new findings in this region.

One of the major characteristic features of the BoB is the enormous freshwater influx (Fig. 1b) that it receives from the river systems [1]. Further, heavy rainfall [2] makes the upper layers of the northern BoB comparatively less saline than the southern part. The northern BoB also experiences high SST in summer which makes the area highly stratified [3]. The seasonal circulation patterns of the BoB are enforced by remote effects from the Indian Ocean along with the monsoonal winds, and freshwater influxes. These exert strong influence on the surface water circulation and stratification with the intention of suppressing the turbulent mixing between surface and cold nutrient-rich subsurface layers [4].

Scientific studies mainly focused on the northern and western part of BoB [5, 6] which are dominated by stratification and detailed how physical processes such as alongshore currents and eddies are able to erode these stratified layers, upwell significant amount of nutrients responsible for blooming in these regions.

However, the northeastern and eastern coast of BoB with largest freshwater fluxes are not much explored

**Corresponding author:** Saswati Deb, Ph.D.; research fields: physical and biological oceanographer. E-mail: saswati.deb@dfo-mpo.gc.ca.

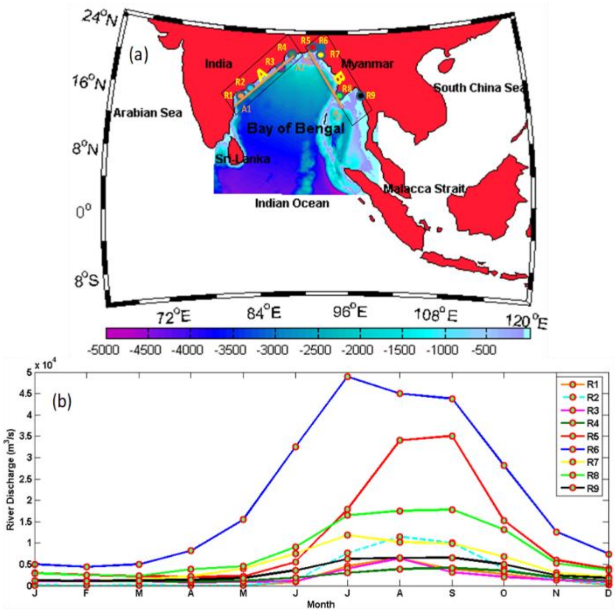


**Fig. 1 The map of Bay of Bengal (a) with bathymetry in meters. The domain is divided into Box A and Box B for further analysis and filled colored circles denote the river discharge point sources along the coast; the orange solid transect line A1A2 (in west coast) and B1B2 (in east coast) illustrates the vertical distribution of chlorophyll concentration in August; (b) the colored lines matching the colored circles along the coast shown above represents the monthly discharge rate. The names of the rivers are listed in Table 1.**

**Table 1 List of rivers included in the model domain.**

| Rivers | Names |
|---|---|
| R1 | River Krishna |
| R2 | River Godavari |
| R3 | River Mahanadi |
| R4 | River Hooghly |
| R5 | River Ganga |
| R6 | River Brahmaputra |
| R7 | River Meghna |
| R8 | River Irrawaddy |
| R9 | River Salween |

in previous studies. The remotely sensed chlorophyll concentration data derived from Sea-viewing Wide Field of view Sensor (SeaWiFS) had been studied [7-9] to hotspot areas rich in chlorophyll concentration. It has been observed that high chlorophyll concentration of more than 1.6 mg/m$^3$ persist along the southeastern part of Sri Lanka dome during July-August. The mechanism that thrives the bloom is the open ocean upwelling driven by Ekman Pumping Velocity (EPV) apart from the wind, earth's rotation along with small-scale cyclonic eddies which dominate these regions. A quality study has been done using Ocean Color Monitor images [10] to demonstrate the impact of cyclonic scale gyre on the growth of bloom in the vicinity of the cyclonic track off the coast of Orissa after the super cyclone in 1999.

Fewer studies [11, 12] exist with limited sampling which addressed the biogeochemical fluxes on a regional scale however, the phytoplankton productivity and its seasonal dynamics are not clear, and the overall information available remains skimpy. However, these studies focused more on the open ocean rather than on coastal dynamics. The coastal dynamic is quite complex with shallow water depth, and freshwater plume cascades with salinity gradients predominate the upper layers. The mixing processes are also regulated by seasonal wind and earth's rotation apart from tides and freshwater fluxes. Now the questions arise how these freshwater fluxes along with intricate coastal processes control the bloom dynamics regionally. These issues remain poorly understood along the east and west coast of the BoB and thus necessary to study.

The prime objective of this work is to understand the consequences of freshwater fluxes on the seasonality of planktons along the coastal sides of the BoB. As the freshwater discharge rate is distinct in western and eastern coast of BoB, so we have divided the BoB into two boxes as illustrated in Fig. 1a. Box A represents west coast of BoB and Box B signifies the east shore of BoB.

This paper emphasized not only on the coastal circulation and physical processes controlling the bloom intensification but also on the freshwater fluxes that determines the spatial and temporal variability of plankton distribution in these coasts. Numerical simulations are carried out by coupling hydrodynamic model with the biogeochemical model, along with coastal current and applied freshwater forcing in

Experiment-1 (Exp1) to analyze the seasonality of bloom; and in Experiment-2 (Exp2), the same coupled model is used but without freshwater forcing. Depending on the potency of the monthly discharge rate of rivers, two more sensitivity experiments are performed.

## 2. Data and Methodology

*2.1 Datasets*

We used climatological monthly mean SeaWiFS Level 3[1] chlorophyll data (for the period of January 2001 to December 2010). The data gaps are assimilated using OA method and SOR algorithm as the initial condition for the model. These satellite-borne sensor data are the derived geophysical variables binned/mapped to a standardized space/time range from different time scales and designed to convey collectively global ocean biological dataset [13]. The principal aim is to measure chlorophyll concentration produced by marine microscopic plants that are phytoplankton. Further, World Ocean Atlas 2013 (WOA13) dataset are used as initial condition for temperature [14], salinity [15], and nitrate [16]. Monthly climatology of SSHA and currents are used from Topography Experiment/Poseidon (TOPEX). The climatological freshwater discharge rates as shown in Fig. 1b (river names are listed in Table 1 and the corresponding location is shown in Fig. 1a) are included in the model. The highest freshwater discharge rate is from River Brahmaputra followed by River Ganga and River Irrawaddy. The monthly mean freshwater discharge rate is obtained by averaging the available monthly runoff over the years from the Global Runoff Data Center [17], Global River Discharge Database [18]. However, due to limited data, the freshwater flux of Rivers Salween and Meghna are accrued from survey study [19]. The average value of freshwater discharge for the River Hooghly [20, 21] is generally more than 3000 $m^3s^{-1}$ during the southwest monsoon.

[1] http://oceancolor.gsfc.nasa.gov/.

*2.2 Model Configuration*

The 3-D hydrodynamic model is coupled with a four-compartment biogeochemical model using Regional Ocean Modeling System (ROMS). ROMS is based on hydrodynamic free-surface terrain-following [22, 23] primitive equations. These equations are calculated based on the Boussinesq approximation and hydrostatic vertical momentum equilibrium in a geocentric rotating frame. The hydrodynamics of the model has been extensively validated with the satellite-borne sensor data [24]. The four-compartment (nitrate as N, phytoplankton as P, zooplankton as Z and detritus as D) biogeochemical model is based on [25, 26]. The governing interaction is kept simpler among the biogeochemical tracers in this biogeochemical model. The equations for the four-compartment biogeochemical model (Fig. 2) can be represented as follows.

$$\frac{\partial [B_i]}{\partial t} = \vec{\nabla}(A\vec{\nabla}B_i) - \vec{V} \bullet \vec{\nabla}B_i + M_i, \tag{1}$$

$$\begin{aligned} M_P &= \mu_P P\left[1-\exp\left(-\frac{\alpha Q_{H_iE} E}{\mu_P}\right)\right]\frac{Q}{Q_{H_iE}}\frac{N}{N+\kappa_N} \\ &-\eta P - \omega P^2 - \mu_Z Z\left[1-\exp(-\lambda P)\right], \end{aligned} \tag{2}$$

$$\begin{aligned} \frac{\partial Q}{\partial t} &= \mu_P\left[1-\exp\left(-\frac{\alpha Q_H E}{\mu_P}\right)\right]\frac{Q}{Q_H} \\ &\times\left\{\frac{N}{N+\kappa_N}\left[Q_L-(\Delta Q)\min\left(\frac{E}{E_k},1\right)\right]-Q\right\}, \end{aligned} \tag{3}$$

$$\begin{aligned} M_Z &= (1-\gamma)\,\mu_Z Z\left[1-\exp(-\lambda P)\right] \\ &-n_1 Z - n_2 Z^2, \end{aligned} \tag{4}$$

$$\begin{aligned} M_D &= \omega P^2 + \gamma\mu_Z Z\left[1-\exp(-\lambda P)\right] \\ &+\varepsilon_1 n_1 Z + \varepsilon_2 n_2 Z^2 - \delta D, \end{aligned} \tag{5}$$

$$\begin{aligned} M_N &= \eta P + (1-\varepsilon_1)n_1 Z + (1-\varepsilon_2)n_2 Z^2 + \delta D \\ &-\mu_P P\left[1-\exp\left(-\frac{\alpha Q_H E}{\mu_P}\right)\right]\frac{Q}{Q_H}\frac{N}{N+\kappa_N}, \end{aligned} \tag{6}$$

$$\mu = \mu_{20} q_{10}^{(T-20)/10}, \tag{7}$$

$$E_S = (1-r)\frac{E_0}{\rho^2}\cos\theta\left[\frac{0.907}{(\cos\theta)^{0.018}}\right]^{\tau_s/\cos\theta}, \tag{8}$$

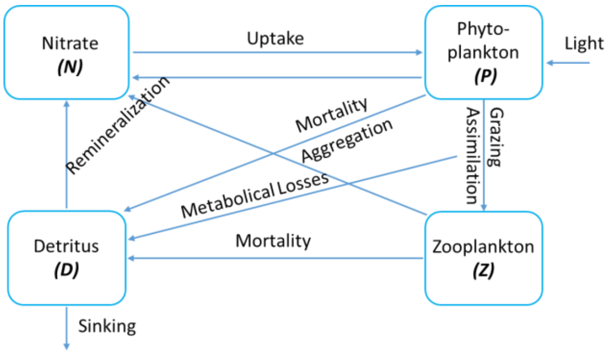


**Fig. 2 Schematic diagram of the four compartment biogeochemical model used to study the pelagic ecosystem of the Bay of Bengal.**

$$\tau_s = 1.40 + 0.136q, \tag{9}$$

$$E(z) = E_S \exp\left[-\kappa_w z + \kappa_c I_C(z)\right], \tag{10}$$

The biogeochemical ($B_i$) tracer in Eq. (1) varies with time. The diffusion factor is defined as $A$, and the velocity vector is represented as $V$. The production minus consumption is denoted as $M_i$. In Eq. (2), the M term for the phytoplankton is expressed in mathematical form. The terms $\mu_p$ and $\mu_z$ stands for maximum growth rates of P and Z respectively and depends on temperature ($q_{10}$) as specified in Eq. (7). The initial slope of the P-E curve is denoted as α. Here, $\eta$ and $\omega$ are P mortality and aggregation rate constant respectively. The term E is the photosynthetically active radiation (PAR) expressed in equations 8 to 10 where the term $I_C(z)$ represents the depth-integrated chlorophyll concentration. Overall, the four terms on the right-hand side of the Eq. (2) represents phytoplankton growth term, mortality rate term, aggregation time, and zooplankton grazing. The ratio of chlorophyll to phytoplankton is represented as $Q$, and the time-rate change of $Q$ depends on the availability N and light as expressed in equation 3. In the equation, $\Delta Q = Q_L - Q_H$, where $Q_L$ is the maximum $Q$ ratio for a low light condition and $Q_H$ is the minimum $Q$ ratio for a high light condition. $\kappa_c$ and $\kappa_w$ are the light attenuation values for the chlorophyll and water. In Eq. (4), the $M_Z$ term for zooplankton includes assimilation and two removal expressions for Z mortality. However, $\lambda$ and $\gamma$ are grazing constant and grazing loss term respectively. The $M_D$ term in Eq. (5) used for detritus contains source term for P aggregation, the expression for grazing loss, the rate for Z mortality and removal rate for D remineralization. The rate of remineralization constant for D is denoted as δ. The $M_N$ term for nitrate in Eq. (6) calculates all remineralization value and the removal by $P$ uptake. The linear and quadratic Z mortality rate constant are represented as $n_1$ and $n_2$ respectively. However, $\varepsilon_1$ and $\varepsilon_2$ are the part of linear and quadratic rate of Z loss respectively that converts to D. At the sea surface, solar irradiance ($E_S$) is calculated in equation 8 and $r$ denotes the cloud coverage term. The solar constant is defined as $E_0$, and the varying distance of sun and earth as $\rho$, moreover $\theta$ as the zenith angle, $q$ as the term for specific humidity.

The model set up for the BoB extends from 76°E to 100°E and 4°N to 24°N with a horizontal resolution of ~10 km and 32 terrain-following vertical levels. The stretching parameters of the model $\theta_s$ = 7.0 and $\theta_b$ = 0.1 are assigned for finer simulation. The bathymetry of the BoB has been extracted from the ETOPO2 dataset which is 2-min topography data [27]. The model inputs are interpolated using OA and assimilated using SOR algorithm and incorporated into the model. For the model simulation, advection of $B_i$ tracers is estimated by the upstream differencing method to control on the production of negative concentrations in areas of extreme gradients. The horizontal diffusivity for the biogeochemical tracers is defined in Eq. (1). The PAR calculation is dependent on zenith angle and carried out at each grid for every time step.

### *2.3 Experimental Design*

In this paper, first two experiments are performed by simulating the coupled numerical model to investigate the predominant role of freshwater forcing on the plankton dynamics. In the first Experiment (Exp1), hydrodynamics coupled with biogeochemical processes including river discharges; in the second

Experiment (Exp2), hydrodynamics coupled with biogeochemical processes without river discharge are simulated. Further sensitivity experiments are performed by doubling (Exp1-FDD) and halved (Exp1-FDH) the freshwater discharges to understand the significant role of the freshwater on blooming.

*2.4 SOR Algorithm*

The successive over-relaxation (SOR) algorithm is an assimilation method used to resolve the set of linear equations, extrapolation derivative of the Gauss-Seidel scheme [28] to prepare the synoptic initial condition. This extrapolation factor is a weighted mean between the preceding value and the calculated Gauss-Seidel value to iterate consecutively for the entire component, here $\bar{X}$ signifies a Gauss-Seidel iterate plus the extrapolation factor. The method decides on a value for $\omega$ that will accelerate the rate of convergence of iterated to the result. SOR algorithm can be written as follows.

$$X_i^{(N)} = \omega \overline{X}_i^{(N)} + (1-\omega) X_i^{(N-1)} \tag{11}$$

*2.5 OA Interpolation*

The Objective Analysis (OA) technique [29] is an interpolation technique which is used to obtain a regular gridded field from the scattered observations. This approach has been used here to develop a high-resolution climatology dataset for chlorophyll, nutrients, temperature, salinity and currents for the BoB which helps in analyzing the new features in comparison to the Levitus climatology and SODA. This new climatology data provides us high resolution and good quality data for all standard depth levels. To prepare a synoptic initial condition, this method was carried out with the *in-situ* profiles, satellite OCM and with the NCEP monthly mean. OA interpolate the fields to the model grid by keeping the dynamical feature information intact and combining the satellite and observed data in an optimal statistical way, which improves its results compared to the direct interpolation method.

*2.6 Skill Assessment*

This method [30] measures the model's accurateness. Based on the agreement between observations and model simulated results, a predictive capability is employed. It is defined as follows.

$$Skill = 1 - \frac{\sum_{i=1}^{N} \left| X_{\text{mod}} - X_{obs} \right|^2}{\sum_{i=1}^{N} \left( \left| X_{\text{mod}} - \bar{X}_{obs} \right| + \left| X_{obs} - \bar{X}_{obs} \right| \right)^2} \tag{12}$$

where, $X$ is the compared variable, $\bar{X}$ is its mean, and the integer $N$ is the total number of measurements.

*2.7 Brief Description of Mixing scheme*

The implementation of river point sources in these studies will help in understanding the influence of freshwater fluxes on the biophysical processes. The vertical mixing in the model is defined by the $k$-$\varepsilon$ turbulence closure scheme coupled with a stability function formula. The quadratic bottom friction is also included in the momentum equation. The parabolic spline method is applied for the vertical derivatives in the numerical simulation. To damp the numerical unsteadiness, the background simulation is directed with horizontal Laplacian diffusion with horizontal assimilation of tracers along the geopotential surfaces.

## 3. Results and Discussion

*3.1 Model Simulated Results and Comparison*

In this section of the paper, we compared the model simulated results with the observations. The seasonality of plankton dynamics is affected by complex hydrodynamics in BoB. We ran the model for the whole domain but downscaled the simulated results into two boxes which include the area of freshwater plumes with a width of 100 to 200 km from the coast. Box A represents the west coast of BoB which is influenced by intricate coastal dynamics, small scale eddies, and the Western Boundary Currents (WBC). Box B is notable for high freshwater discharge, strong estuarine circulation, boundary currents and high stratification. Therefore, these boxes contribute significant amount of seasonal bloom. Besides, these physical processes prevailing in the north, the southern BoB is influenced by momentous water mass exchanges with the Arabian Sea and the Indian Ocean from the south and with the Pacific Ocean and the South China Sea via Malacca Strait from the southeast. Therefore, the coupled model is first validated with the remote sensing data for the physical processes that are linked to influence plankton dynamics and then biogeochemical aspects of the BoB are compared.

The modeled Sea Surface Height Anomalies (SSHA) is compared with TOPEX, Sea Surface Temperature (SST) with Advanced Very High Resolution Radiometer (AVHRR), Mixed Layer Depth (MLD) and 20°C isotherm depth (D20) with Array of Real-time Geostrophic Oceanography (ARGO).

The correlation coefficient comparison map for SST shows higher coefficient on the western side of BoB compared to the eastern BoB (Fig. 3a). Moreover, the correlation value of SSHA is in good agreement along the coast compared to the central BoB (Fig. 3c) whereas for MLD (Fig. 3e) and D20 (Fig. 3g) the correlation value is higher on the northern and southern BoB. The correlations with the observations are above 0.9 for SST, 0.76 for MLD and above 0.5 for SSHA and D20. The comparison showed reasonable correlations between modeled outputs and observations, and thus ascertained that the model is capable of simulating the observed seasonal variability.

The model skill assessment map for SST showed good agreement with AVHRR and the mean skill calculated for the whole domain is 0.94 (Fig. 3b). The model skill map for SSHA showed good score at the west coast, however, there are some areas with less score which indicates that eddies are not produced at the exact location as of the observation (Fig. 3d). The model skill for MLD over the domain showed good accord, and the mean skill is 0.80 (Fig. 3f) however, for the D20 the model scored better at the west coast compared to the rest part of the basin (Fig. 3h). To produce a statistical summary, the mean value of correlation and skill are also compared in the Taylor diagram (Fig. 4).

These systematic model-data comparisons determined how well the model replicates the different physical aspects of the observed variability.

Further, model simulated surface currents (Fig. 5) with varying SSHA revealed the formation of two anticyclonic eddies with two distinct nuclei on the western side of BoB along with the formation of WBC during March. SSHA derived from TOPEX along with geostrophic current also shows good agreement with the model and distinguishable two anticyclonic eddies in March. On the western coast of BoB, the downwelling zones are identified illustrating positive SSHA which is mainly due to strong negative wind stress curl in these regions. In the month of August, four cyclonic eddies are identified from the model simulation. The location of these cyclonic eddies are approximately centered at 83.42°E, 16.25°N; 85.6°E, 18.12°N; 88.71°E, 18.25°N; and 92.3°E, 17.65°N (Fig. 5). From the SSHA illustration, the upwelled water moving along the coast are distinguishable in both model and TOPEX. The anticyclonic eddy centered at the western boundary of BoB shifts northward. This shifting reduces the water mass transportation to some extent towards the north. The modeled SSHA can detect the upwelled water associated with the cyclonic eddy at the mouth of Rivers Krishna and Godavari in August. However, the cyclonic eddy formed at the mouth of River Mahanadi is weaker compared to the above described eddies. From the model simulation, it is also observed that a cyclonic gyre prevails in the northern BoB whereas an anticyclonic gyre in the southern BoB. The eastern boundary currents are associated with small scale cyclonic eddies near the mouth of River Irrawaddy approximately centered at 95.41°E, 14.01°N and 97.12°E, 10.83°N respectively.

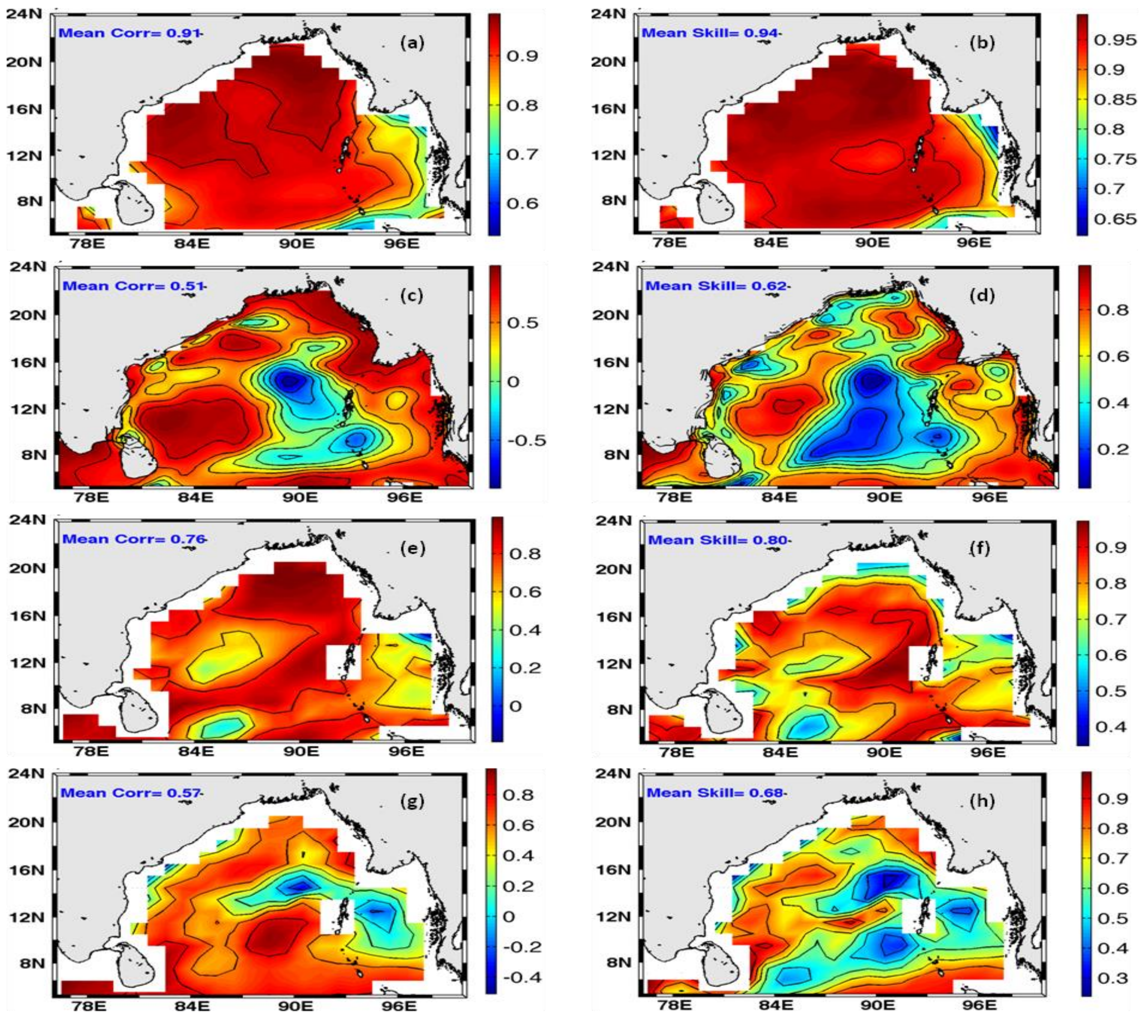


**Fig. 3 The correlation map for (a) SST, (c) SSHA, (e) MLD, and (g) D20. The skill map for (b) SST, (d) SSHA, (f) MLD, and (h) D20. The mean values of the correlation coefficient and skill assessment are calculated and included inside each box.**

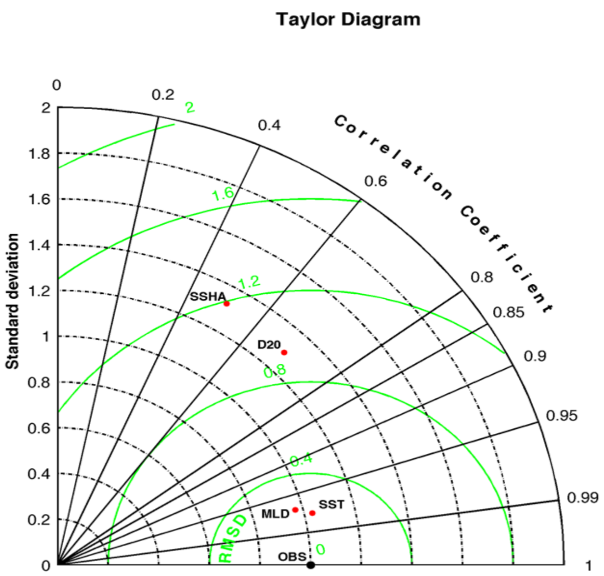


**Fig. 4 Normalized Taylor diagram for model simulated SSHA, SST, MLD and D20.**

In November, the cyclonic eddy approximately centered at 82.11°E, 9.71°N towards the northeast of Sri-Lanka dome, elongates to make the East India Coastal Current (EICC) stronger and flow continuously along the western boundary of BoB. The model simulated EICC flowing southward along the coast with a positive SSHA is also observed from TOPEX. The strong upwelled water along the western boundary of BoB is depicted both in model simulation and TOPEX. However, the eastern boundary current is found not along the coastline but shifted towards the Andaman and Nicobar Islands due to the subsistence of few significant anticyclonic eddies with positive SSHA observed from the simulation and TOPEX.

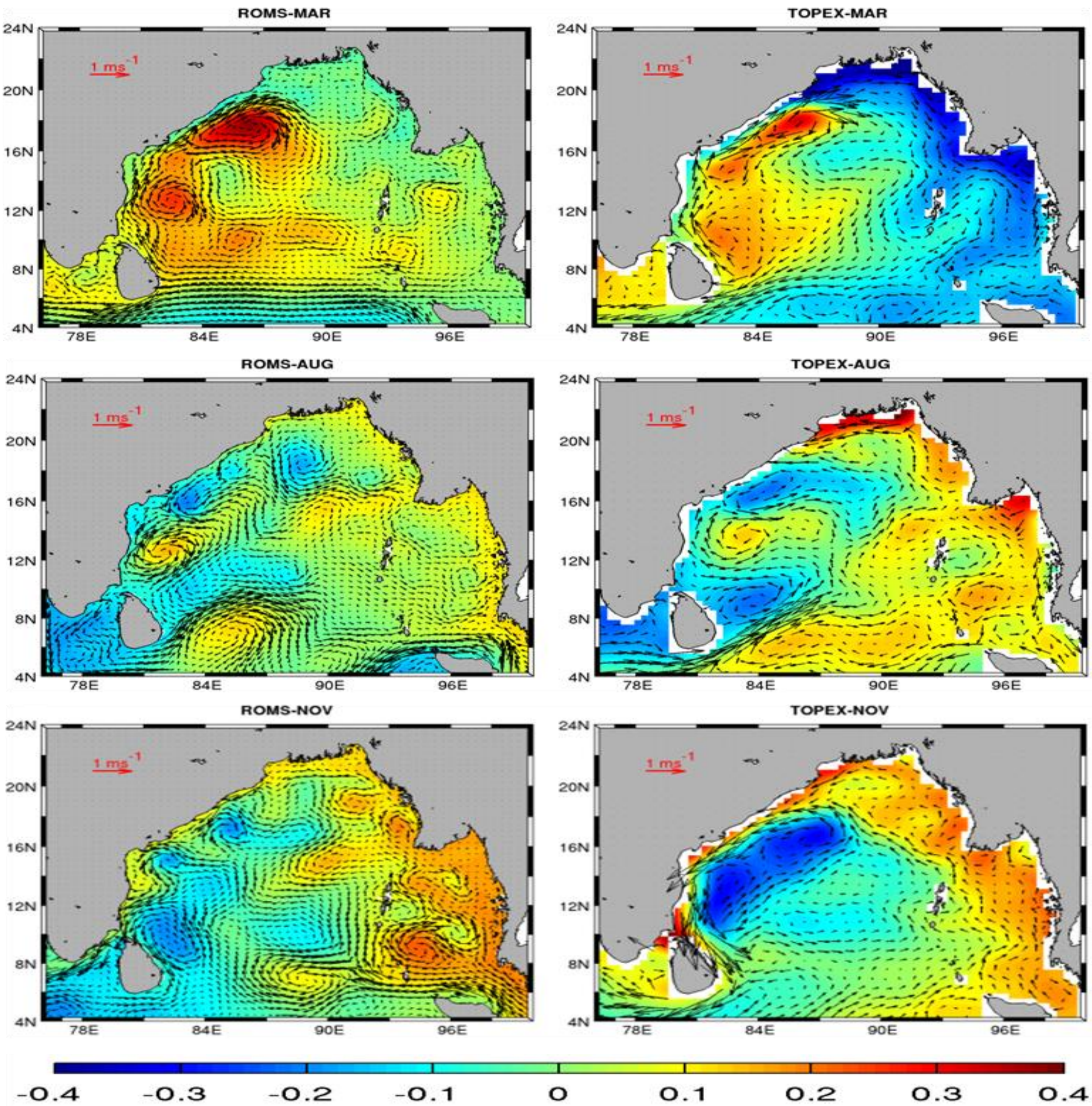


**Fig. 5 Monthly climatology of surface currents (vectors) and SSHA (color shaded) for March, August, November from the model simulations (left panel) and TOPEX (right panel).**

*3.2 Seasonal Variation of Plankton Dynamics*

The model generates intense bloom patches around the nearshore upwelling coastal regions of the BoB (Fig. 6). The model simulated chlorophyll concentration is compared with the ten-year monthly mean SeaWiFS chlorophyll surface data. The RMSE calculated (in Table 2) between the SeaWiFS and model simulated chlorophyll concentration shows reasonable agreement. The skill assessment values calculated for the months March, August and November are 0.78, 0.70 and 0.84 respectively. Therefore, the modeled chlorophyll concentration is in good agreement with the SeaWiFS data. However, in the model simulation, over-predicted blooms are observed along the coastal shelf which may results from high nutrient discharge from river runoff as observed in August-September and/or coastal upwelling leading to increased nutrient in the upper layers supporting the growth of bloom. Another possible reason for the less skill assessment values in August is due to the lack of SeaWiFS chlorophyll data near the coast and open sea which is caused as a result of monsoonal cloud cover. On the other hand, observed data are inadequate near the coast to provide a concrete explanation for the hypothesis. However, the annual mean RMSE calculated between SeaWiFS data and modeled chlorophyll concentration for the BoB is 0.42 which signifies the model output is in good agreement with the observed data. Furthermore, box-wise detailed RMSE comparison is done in Table 2. The onset of blooming time in the BoB differs from east to west. The squat values of chlorophyll concentration are found in the open ocean. Along the coast, complex dynamics such as riverine-coastal circulation enhances the bloom. It is found that the eddy like structure generated near the freshwater discharge point is associated with nutrient enriched cool waters. The area along the coast towards the head of the BoB is pre-dominated with high chlorophyll concentration bloom (above 2 mg/m$^3$) due to the coastal upwelling. The maximum blooms are oomph by high nitrate associated with coastal upwelling along with proper light conditions. Even though we studied all the months, however, in this paper, seasonal variability in March, August, and November are highlighted due to the unique coastal dynamics influencing the bloom.

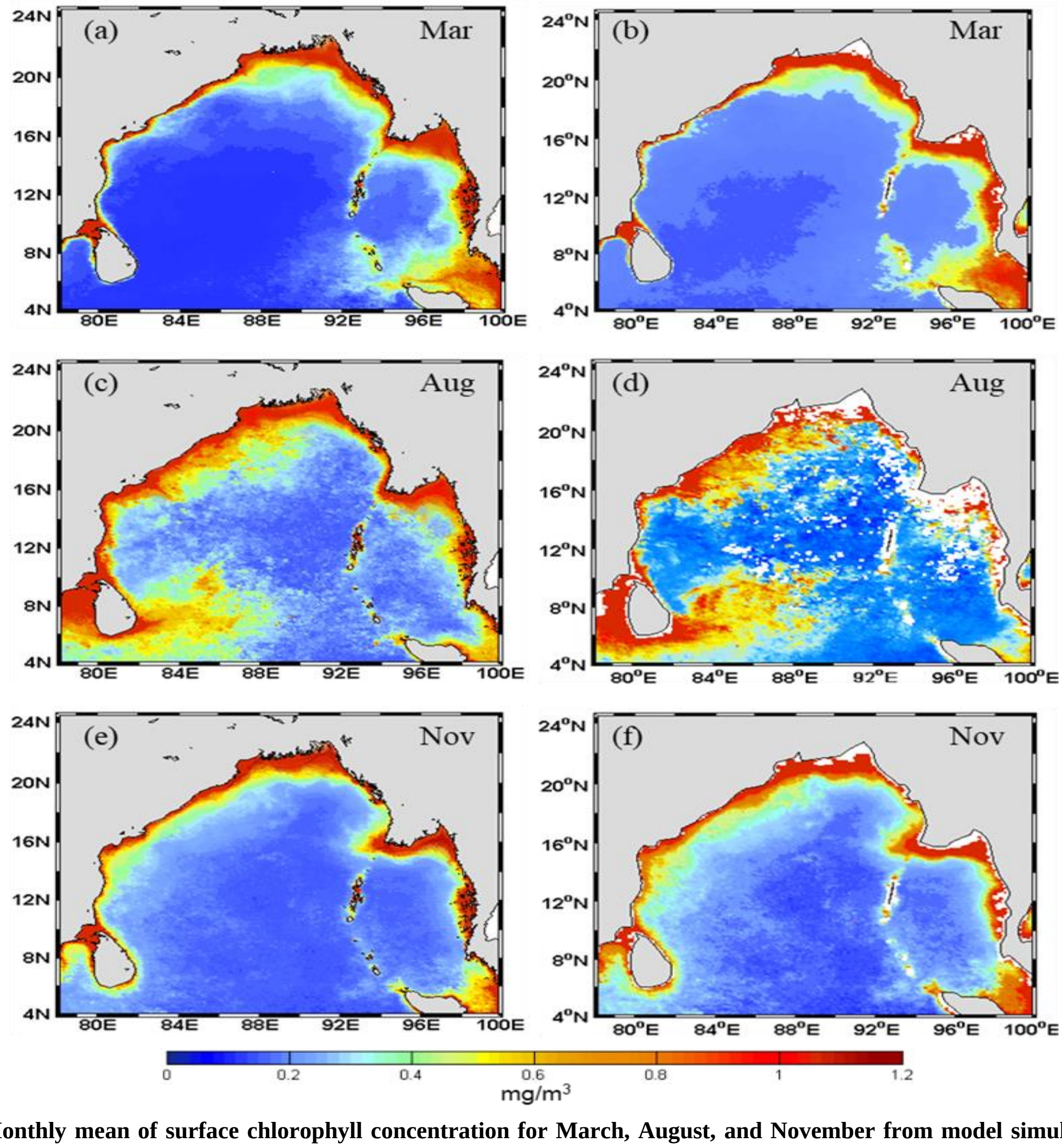


**Fig. 6 Monthly mean of surface chlorophyll concentration for March, August, and November from model simulation (left panel) and SeaWiFS (right panel).**

**Table 2 Comparison of RMSE calculated.**

| Box-wise | Obs vs Exp-1 (Chloro-phyll in mg/m$^3$) | Obs vs Exp-1 (Nitrate in μmol/l) | Exp-1 vs Exp-2 (Chloro-phyll in mg/m$^3$) | Exp-1 vs Exp-2 (Nitrate in μmol/l) | Exp-1 vs Exp-2 (Zoo-plankton in mg/m$^3$) |
|---|---|---|---|---|---|
| Box A | 0.08 | 0.05 | 0.07 | 0.05 | 0.06 |
| Box B | 0.08 | 0.07 | 0.07 | 0.08 | 0.04 |

Apart from analyzing the whole domain, box-wise illustration further distinguishes the seasonal variation of chlorophyll (Fig. 7) and nitrate concentration (Fig. 8) between the two coasts. Both observed and modeled monthly mean surface chlorophyll concentration showed similar trend during February-March-April, in Box B (Fig. 7b) and almost twice the concentration in Box A (Fig. 7a). A peak chlorophyll concentration is observed in Box A during September with a slight deviation (model over-predicted value). However, two peaks of chlorophyll concentration are observed in Box B, one at March and another in September. Therefore, comparing the two boxes, it can be revealed that the bloom intensifies in March followed by September along the eastern coast of BoB whereas at west coast high bloom predominates in August-September. However, both the boxes showed a low concentration of chlorophyll during May-June. Also the modeled surface nitrate concentrations of the two boxes are compared with WOA13. In Box A (Fig. 8a), a peak is noticed in September whereas in Box B (Fig. 8b) two peaks are observed during March and September with a maximum value of nitrate in September. These high values of nitrate are observed along the east coast where discharges from the Rivers Ganga, Brahmaputra, Meghna and Irrawaddy are large. Fig. 7a and 8a depicts how the nitrate is used up by planktons in March leading to increased bloom. In the western coast of BoB, apart from freshwater fluxes, WBC plays a significant role in the transport of nitrate to the upper surface from nitracline (sub-surface layers) and is consistent with survey [6]. This strong WBC flow northward and extends up to 20°N and then becomes weak due to the distance between the two anticyclonic eddies. These physical processes play an important role in the blooming time which differs among the coasts.

The blooming time varies from west to east in the BoB. In March-April, the western BoB is associated with anticyclonic eddies making it downwelling zones and the low freshwater discharge explained that the phytoplankton bloom is limited by nitrate. On the northeastern and eastern coast of BoB, the onset of summer phytoplankton bloom is noticed. An increased level of bloom is observed near the mouth of Rivers Ganga-Brahmaputra-Meghna and Irrawaddy-Salween. These inferred that freshwater fluxes associated with nutrients thrives the onset of blooming in this region. However, the growth of phytoplankton bloom in this region is limited by the availability of nitrate. During the southwest monsoon, particularly in August-September, peaks of phytoplankton bloom are observed in both the Boxes A and B. During this season, the blooming is limited mainly by light. In August, both the coasts are dominated by cyclonic eddies and high freshwater fluxes; however, the western BoB (Box A) is mostly influenced by strong cyclonic eddies and eastern BoB (Box B) by massive freshwater fluxes. These cyclonic eddies increased the rate of supply of nutrient from subsurface nutricline layers to the upper layers of sea surface by eroding the stratified layers especially in the northern BoB. Surface and subsurface mixing further enhanced the blooming.

In Box B, the cyclonic gyre formed at the mouth of Rivers Irrawaddy-Salween gaggled the subsurface nutrient-rich cooler waters to the surface layers. The cyclonic gyre associated with few more cyclonic eddies moving northwards further influence these physical processes. In the vicinity of the Ganga-Brahmaputra-Meghna deltaic zone, the stratification is eroded by upwelling which is induced by strong monsoonal wind. In November, the Box B is predominated by anticyclonic eddies with currents flowing northward and then advected towards the Box A. The cyclonic eddies prevailed in Box A along with strong EICC flowing southward transported upwelled nutrient-rich waters to the surface layers thereby enhancing phytoplankton bloom.

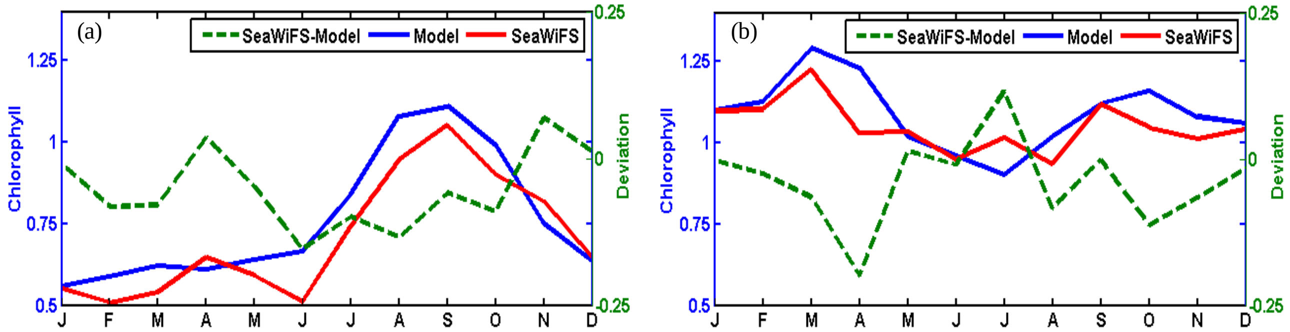


**Fig. 7 Monthly comparison of surface chlorophyll concentration (mg/m$^3$) between the model and SeaWiFS for (a) Box A and (b) Box B.**

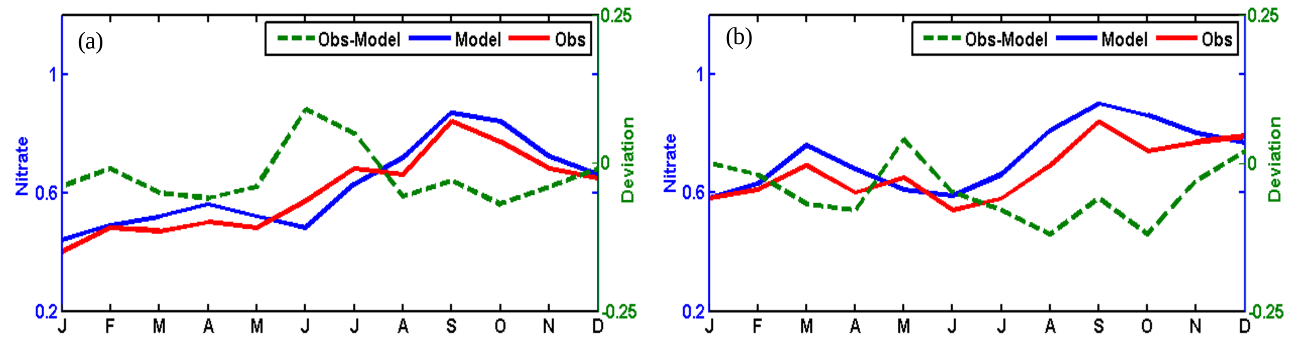


**Fig. 8 Monthly comparison of surface nitrate (μmol/l) between the model and WOA13 for (a) Box A and (b) Box B.**

### *3.3 Sensitivity Analysis*

Sensitivity experiments are carried out to determine the potency of the freshwater fluxes on the growth of planktons by varying the discharge rates. Results illustrated in Fig. 7 and 8 are considered as Exp1 (the control run). Based on control run, Exp2 is simulated without river discharge considering other physical and biogeochemical conditions same as Exp1.

From the Fig. 9a, it is observed that the bloom peak (Exp2) gets retarded from August compared to Exp1. However, in Box B [Fig. 9b], the two phytoplankton peaks (Exp2) deterred in March and October compared to Exp1.

The seasonal variation of surface nitrate in Exp2 (Fig. 10) follows the similar trend as Exp1 with a maximum deviation observed in July and September. Model-model comparison of zooplankton concentration (Fig. 11) is also revealed. Zooplankton concentration is found to be quite retarded in Box A during August-September which explains that the growth is dependent on nutrients and also influenced by freshwater fluxes. In addition, the grazing rate is also dependent on the phytoplankton growth rate.

Model simulated zooplankton distribution (Exp1) is high at the western coast of the BoB in August-September and also in the vicinity of the coastal areas with high freshwater discharges and well matched with the existing study [31, 32]. However, in Box B, the zooplankton growth peaks in March (both for Exp1 and Exp2) and October (Exp1).

However, further sensitivity experiments are conducted based on Exp1 by doubling the freshwater discharge (Exp1-FDD) and halved the discharge rate (Exp1-FDH). The annual mean of chlorophyll concentration calculated (Table 3) based on Exp1 with doubling the freshwater discharge rate (Exp1-FDD) showed that the intensification of bloom increased by 60 percent in Box B and 65 percent in Box A. Again, based on Exp1, the model simulation with 50 percent reduced freshwater discharge rate (Exp1-FDH) showed reduced bloom growth by 25 percent in Box B and 15 percent in Box A. The experimental results suggested that the freshwater plays a dominant role but nonlinearly related to plankton growth. In Table 3, the freshwater discharges are denoted as FD.

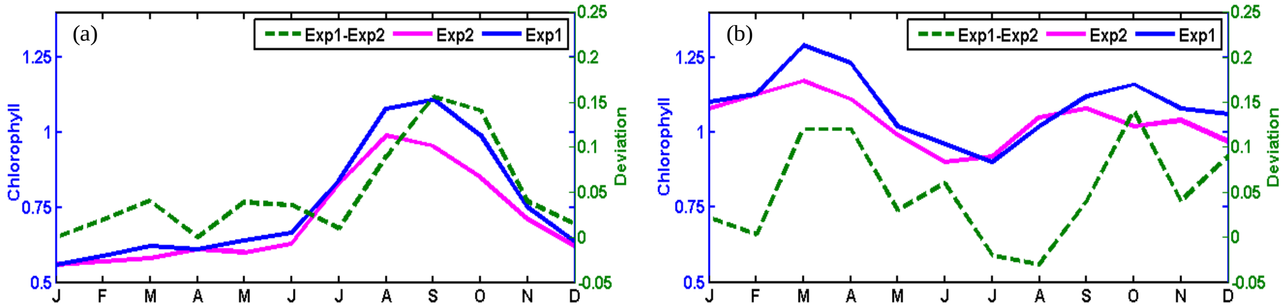


**Fig. 9 Monthly model-model comparison of surface chlorophyll concentration (in mg/m$^3$) for (a) Box A and (b) Box B.**

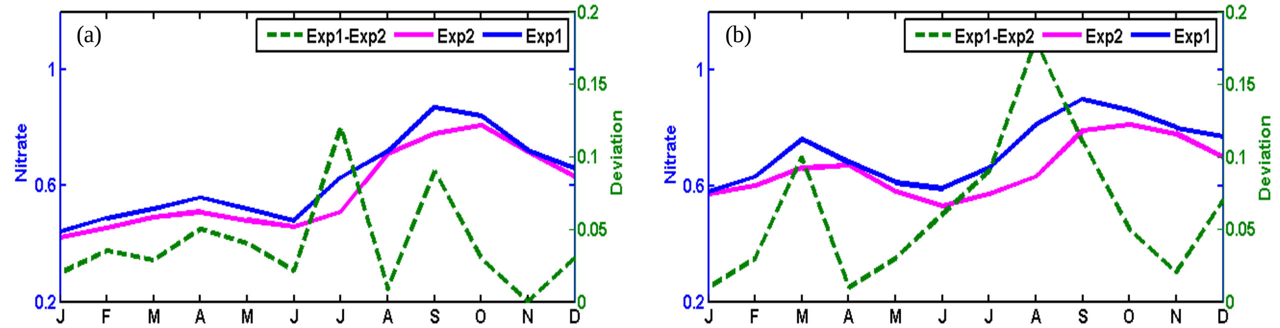


**Fig. 10 Monthly model-model comparison of surface nitrate concentration (in μmol/l) for (a) Box A and (b) Box B.**

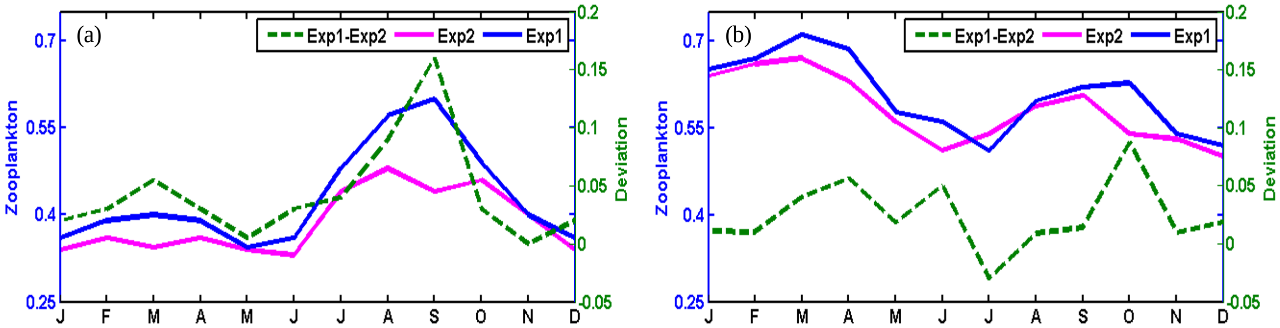


**Fig. 11 Monthly model-model comparison of surface zooplankton concentration (in mg/m$^3$) for (a) Box A and (b) Box B.**

**Table 3 Model sensitivity experiments performed**

| Experiment | Description of Experiments Performed | Annual mean (Chlorophyll in mg/m$^3$) |
|---|---|---|
| Box A Exp1 | Model simulation with observed FD for Box A | 0.76 |
| Box A Exp1-FDD | Model simulation with doubled FD for Box A | 1.25 |
| Box A Exp1-FDH | Model simulation with halved FD for Box A | 0.65 |
| Box B Exp1 | Model simulation with observed FD for Box B | 1.09 |
| Box B Exp1-FDD | Model simulation with doubled FD for Box B | 1.74 |
| Box B Exp1-FDH | Model simulation with halved FD for Box B | 0.81 |

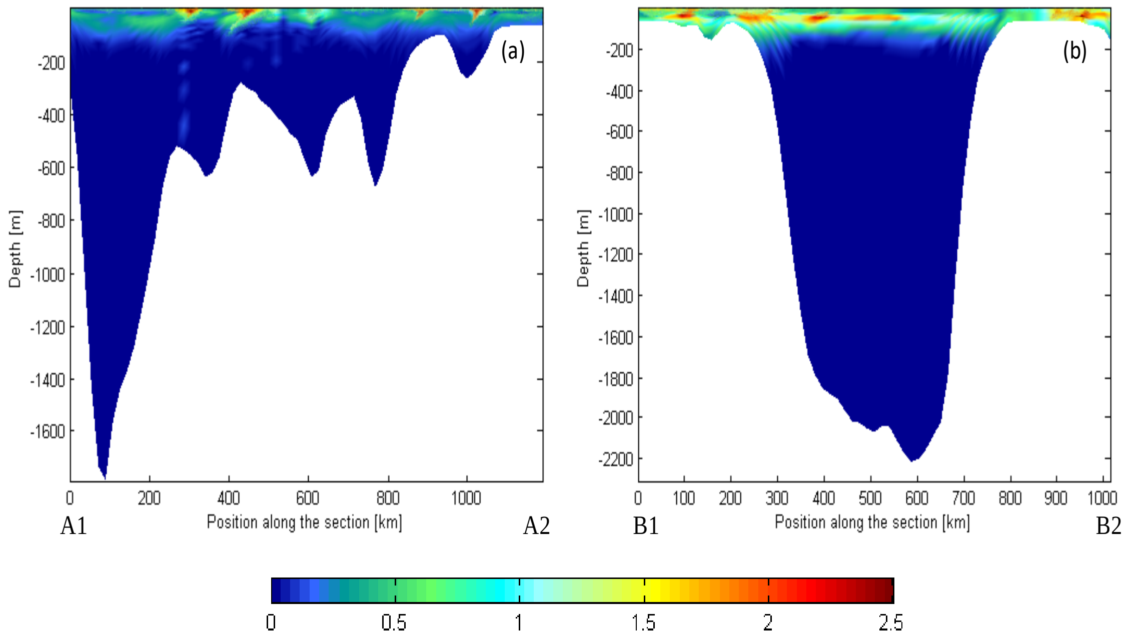


**Fig. 12 Vertical section of chlorophyll concentration (in mg/m$^3$) along the transect (a) A1A2 and (b) B1B2 in August.**

## 4. Conclusions

The model simulated seasonal variations of chlorophyll concentrations in BoB reasonably reproduces similar patterns with the remotely sensed SeaWiFS data. The hydrodynamics of the model are also thoroughly validated with the satellite-borne data. Though the simulated results can resolve most of the known biophysical response of the BoB in reasonable agreement with the earlier study [33, 34] and remotely sensed data, however, some new features are also observed from the numerical simulations. The model simulated chlorophyll concentration distinguishes the BoB into two seasonal productive regions.

From the biogeochemical results, a sharp contrast of vertical distribution of chlorophyll concentrations between Box A and Box B are observed (Fig. 12). The blooming time for Box A is around August-September whereas for Box B the patches of chlorophyll concentration peaked around March-April and September-October. The freshwater fluxes are high in Box B compared to Box A. In Box B, the formation of freshwater plume from River Ganga, Brahmaputra, and Irrawaddy during April-May-June retarded the growth of plankton. However, the growth of plankton in September are driven by unique physical processes. The study revealed that two significant peak of phytoplankton blooms are observed (in March and September) along the east coast of BoB and a peak in September along the west coast is driven by freshwater fluxes, monsoonal wind and complex riverine-coastal circulation associated with cyclonic eddies. Zooplankton concentration peaked in August-September in Box A and establish quite retarded growth in Exp2 which meant that the growth is potentially controlled by freshwater discharge. Also the grazing rate is dependent on the phytoplankton growth rate. Sensitivity experiments are further performed based on Exp1, by doubling the freshwater discharge (Exp1-FDD), increased the bloom growth by 65 percent in Box A and 60 percent in case of Box B. However, reducing the freshwater discharge by 50 percent (Exp1-FDH) reduced the bloom intensification by 15 percent in case of Box A and 25 percent in case of Box B, signifies that the freshwater plays a dominant role but nonlinearly related to plankton dynamics. The model overestimated surface chlorophyll concentrations at some upwelled nearshore coastal regions of BoB compared to the observation. However, a possible reason for the incongruity is inadequate data to accurately quantify the concentration at the nearshore, and also emphasized to improve the parameters of turbulent mixing scheme in the model.

## References

[1] Subramanian, V. (1993). "Sediment load of the Indian Rivers." *Current Science* 64: 928-930.

[2] Venkateswaran, S. V. (1956). "On Evaporation From the Indian Ocean." *Indian Journal of Meteorological Geophysics* 7: 265-284.

[3] Narvekar, J., and Prasanna Kumar, S. (2006). "Seasonal Variability of the Mixed Layer in the Central Bay of Bengal and Associated Changes in Nutrients and Chlorophyll." *Deep-Sea Research I* 53: 820-835.

[4] Shetye, S. R., Gouveia, A. D., Shankar, D., Shenoi, S. S. C., Vinayachandran, P. N., Sundar, D., Michael, G. S., and Nampoothiri, G. (1996). "Hydrography and Circulation in the Western Bay of Bengal During the Northeast Monsoon." *Journal of Geophysical Research* 101: 114011-14025.

[5] Gomes, H. R., Goes, J. I., and Saino, T. (2000). "Influence of Physical Processes and Freshwater Discharge on the Seasonality of phytoplankton Regime in the Bay of Bengal." *Continental Shelf Research* 20: 313-330.

[6] Shetye, S. R., Gouvela, A. D., Shenoi, S. S. C., Sundar, D., Michael, G. S., and Nampoothiri, G. (1993). "The Western Boundary Current of the Seasonal Subtropical Gyre in the Bay of Bengal." *Journal of Geophysical Research* 98: 945-954.

[7] Deb, S., and Chakraborty, A. (2016). "Numerical Analysis of the Biogeochemical Parameters in the Bay of Bengal." *Journal of Shipping and Ocean Engineering* 6: 135-148.

[8] Deb, S., and Das, B. (2020). "Numerical Simulation of Plankton Dynamics and Its Sensitivity to Seasonal Variations in Freshwater Forcing." In: *IEEE Xplore of Geoscience and Remote Sensing Symposium*, pp. 5889-5892.

[9] Murtugudde, R. G., Signorini, S. R., Christian, J. R., Busalacchi, A. J., McClain, C. R., and Picaut, J. (1999). "Ocean Color Variability of the Tropical Indo-Pacific Basin Observed by SeaWiFS During 1997-1998." *Journal of Geophysical Research* 104: 351-366, doi: 10.1029/1999JC900135.

[10] Nayak, S. R., Sarangi, R. K., and Rajawat, A. S. (2001). "Application of IRS-P4 OCM Data to Study the Impact of Cyclone on Coastal Environment of Orissa", *Current Science* 80: 1208-1213.

[11] Ittekkot, V., Nair, R. R., Honjo, S., Ramaswamy, V., Bartsch, M., Manganini, S., and Desai, B. N. (1991). "Enhanced Particle Fluxes in Bay of Bengal Induced by Injection of Fresh Water", *Nature* 351: 385-387.

[12] Schafer, P., Ittekkot, V., Bartsch, M. and Nair, R. R. (1996). "Fresh Water Influx and Particle Flux Variability in the Bay of Bengal." In: *Particle Flux in the Ocean*, Wiley, New York, pp. 271-292.

[13] NASA (2014). "Goddard Space Flight Center, Ocean Biology Processing Group, Sea-viewing Wide Field-of-view Sensor (SeaWiFS) Ocean Color Data." NASA OB.DAAC, Greenbelt, MD, USA, doi: 10.5067/ORBVIEW-2/SEAWIFS_OC.2014.0.

[14] Locarnini, R. A., Mishonov, A. V., Antonov, J. I., Boyer, T. P., Garcia, H. E., Baranova, O. K., Zweng, M. M., Paver, C. R., Reagan, J. R., Johnson, D. R., Hamilton, M., and Seidov, D. (2013). "*World Ocean Atlas 2013, Volume 1: Temperature*." S. Levitus (Ed.), A. Mishonov (Technical Ed.); NOAA Atlas NESDIS, pp. 40, 73.

[15] Zweng, M. M., Reagan, J. R., Antonov, J. I., Locarnini, R. A., Mishonov, A. V., Boyer, T. P., Garcia, H. E., Baranova, O. K., Johnson, D. R., Seidov, D., and Biddle, M. M. (2013). "*World Ocean Atlas 2013*, *Volume 2: Salinity*." S. Levitus (Ed.), A. Mishonov (Technical Ed.); NOAA Atlas NESDIS, pp. 39, 74.

[16] Garcia, H. E., Locarnini, R. A., Boyer, T. P., Antonov, J. I., Baranova, O. K., Zweng, M. M., Reagan, J. R., and Johnson, D. R. (2014b). "*World Ocean Atlas 2013, Volume 4: Dissolved Inorganic Nutrients (Phosphate, Nitrate, Silicate*)." S. Levitus (Ed.), A. Mishonov (Technical Ed.); NOAA Atlas NESDIS, pp. 25, 76.

[17] Fekete, B. M., Vorosmarty, C. J., and Grabs, W. (2000). "Global, Composite Runoff Fields Based on Observed River Discharge and Simulated Water Balances." Documentation for UNHGRDC Composite Runoff Fields, v.1.0. Global Runoff Data Center, Koblenz, Germany.

[18] Vorosmarty, C. J., Fekete, B. M., and Tucker, B. A. (1998). "Global River Discharge Database (RivDis)", V. 1.1.

[19] Jana, S., Gangopadhyay, A., and Chakraborty, A. (2015). "Impact of Seasonal River Input on the Bay of Bengal Simulation." *Continental Shelf Research* 104: 45-62.

[20] Mukhopadhyay, S. K. (2007). "The Hooghly Estuarine System, NE Coast of Bay of Bengal, India." In: *Proceeding in Workshop on Indian Estuaries*, Goa: NIO, pp. 1–26.

[21] Deb, S., and Chakraborty, A. (2015). "Simulating the Effects of Tidal Dynamics on the Biogeochemistry of the Hooghly Estuary." *IEEE Journal of Selected Topics in Applied Earth Observations and Remote Sensing* 8: 130-140.

[22] Haidvogel, D. B., Arango, H. G., Hedstrom, K. A., Beckmann, P., Malanotte-Rizzoli, and Shchepetkin, A. F. (2000). “Model Evaluation Experiments in the North Atlantic Basin: Simulations in Nonlinear Terrain-Following Coordinates.” *Dynamics of Atmospheres and Oceans* 32: 239-281.

[23] Shchepetkin, A. F., and McWilliams, J. C. (2005). “The Regional Ocean Modeling System (ROMS): A Split-Explicit, Free-Surface, Topography-Following Coordinates Ocean Model.” *Ocean Modelling* 9: 347-404.

[24] Sil, S. (2012). “High Resolution Ocean State Simulations in the Bay of Bengal using the Regional Ocean Modeling System (ROMS).” PhD thesis, Indian Institute of Technology, Kharagpur, India.

[25] Fasham, M. J. R., Ducklow, H. W., and McKelvie, S. M. (1990). “A Nitrogen-Based Model of Plankton Dynamics in the Ocean Mixed Layer”, *Journal of Marine Research* 48: 591-639.

[26] Liu, K. K., Chao, S. Y., Shaw, P. T., Gong, G. C., Chen, C. C., and Tang, T. Y. (2002). “Monsoon-Forced Chlorophyll Distribution and Primary Production in the South China Sea: Observations and a Numerical Study.” *Deep-Sea Research I* 49: 1387-1412.

[27] Smith, W. H. F., and Sandwell, D. T. (1997). “Global Sea Floor Topography From Satellite Altimetry and Ship Depth Soundings”, *Science* 277: 1956-1962.

[28] David, Y. M. (1950). “Iterative Methods for Solving Partial Difference Equations of Elliptical Type.” PhD thesis, Harvard University, Cambridge, MA.

[29] Lermusiaux, P. F. J. (1999). “Data Assimilation via Error Subspace Statistical Estimation, Part II: Middle Atlantic Bight Shelfbreak Front Simulations Validation”, *Monthly Weather Review* 1278: 1408-1432.

[30] Wilmott, C. J. (1981). “On the Validation of Models.” *Physical Geography* 2: 184-194.

[31] Rakhesh, M., Raman, A. V., Kalavati, C., Subramanian, B. R., Sharma, V. S., Sunitha Babu, E., and Sateesh, N. (2008). “Zooplankton Community Structure Across an Eddy-Generated Upwelling Band Close to a Tropical Bay-Mangrove Ecosystem.” *Marine Biology* 154: 953-972.

[32] Fernandes, V., and Ramaiah, N. (2009). “Mesozooplankton community in the Bay of Bengal (India): Spatial Variability During the Summer Monsoon.” *Aquatic Ecology* 43: 951-963.

[33] Vinayachandran, P. N. (2009). “Impact of Physical Processes on Chlorophyll Distribution in the Bay of Bengal.” *Geophysical Monograph Series*: 71-86.

[34] Ritthirong, P., Pirote, N., and Natinee, S. (2008). “*Distribution of Nutrients in the Bay of Bengal, The Ecosystem-Based Fishery Management in the Bay of Bengal*”, pp. 33-44.